Turbulent Wake of a Flat Plate

V. C. Patel* and H. C. Chen†
University of Iowa, Iowa City, Iowa

The Reynolds-averaged Navier-Stokes equations, together with the equations of the k-ϵ model of turbulence, are solved numerically in a large computational domain surrounding the trailing edge of a flat plate. The solutions extend from the boundary layer on the plate through the interaction zone around the trailing edge into the far wake. The results are compared with experiments, Alber's theory of near wake, and solutions obtained previously with boundary-layer equations. Satisfactory agreement is found in all regions except that the rate of growth of the far wake is underestimated. The latter result reconfirms the well-known defect of the k-ϵ model.

I. Introduction

THE flow at the trailing edge of a flat plate provides a simple yet effective test case for calculation methods because it involves the evolution of a well-documented boundary layer into an equally well-documented free shear layer through a region of viscous-inviscid interaction due to the discontinuity in boundary conditions at the trailing edge. The authors have recently presented numerical solutions of the Navier-Stokes equations for the laminar case.[1] An important observation made there is that solution domains much larger than those used in previous studies must be employed to capture completely all the details of such flows.

Available experimental information on the turbulent wake of a flat plate was reviewed by Ramaprian et al.[2] They suggested that the wake can be divided into three regions: the very near wake, in which the sublayers of the boundary layer are consumed, an intermediate region, in which the logarithmic layers are destroyed, followed by the asymptotic, small-defect, far wake, in which the mean flow and turbulence reach a state of self-preservation. In a contemporary study, Patel and Scheuerer[3] presented solutions of the boundary-layer equations with the k-ϵ turbulence model and showed that such calculations predict the important features of the flow in the near wake but fail to predict correctly either the asymptotic growth rates or the shapes of the velocity, shear-stress, and turbulent kinetic-energy profiles in the far wake. This rather mixed performance was attributed to deficiencies that develop in the turbulence model in the far wake.

In the present paper, we reconsider the turbulent trailing-edge problem with the objective of including the viscous-inviscid interaction and determining the influence of the terms neglected in the boundary-layer equations. The numerical method of Ref. 1 is employed to solve the Reynolds-averaged Navier-Stokes equations, together with the equations of the k-ϵ model of turbulence. Two different treatments of the flow close to the wall are considered, namely, a two-point wall-function approach, and a new procedure in which the k-ϵ model is combined with a simple eddy-viscosity distribution for the wall region in a two-layer formulation. It is found that the latter provides a more detailed description of the flow in the near wake and offers a better prospect for further generalizations to more complex flows.

Received May 19, 1986; revision submitted Oct. 17, 1986.

*Professor of Mechanical Engineering, Iowa Institute of Hydraulic Research. Member AIAA.
†Assistant Research Scientist, Iowa Institute of Hydraulic Research. Member AIAA.

II. Equations and Turbulence Models

In Cartesian (x,y) coordinates, with x measured along the plate from the trailing edge and y normal to it, the complete Reynolds-averaged Navier-Stokes equations for a two-dimensional incompressible flow are:

$$\frac{\partial U}{\partial t}+U\frac{\partial U}{\partial x}+V\frac{\partial U}{\partial y}+\frac{\partial}{\partial x}(p+\overline{uu})+\frac{\partial}{\partial y}(\overline{uv})-\frac{1}{R}\left(\frac{\partial^2 U}{\partial x^2}+\frac{\partial^2 U}{\partial y^2}\right)=0 \tag{1}$$

$$\frac{\partial V}{\partial t}+U\frac{\partial V}{\partial x}+V\frac{\partial V}{\partial y}+\frac{\partial}{\partial x}(\overline{uv})+\frac{\partial}{\partial y}(p+\overline{vv})-\frac{1}{R}\left(\frac{\partial^2 V}{\partial x^2}+\frac{\partial^2 V}{\partial y^2}\right)=0 \tag{2}$$

where (U,V) and (u,v) are, respectively, the mean and fluctuating velocity components in the (x,y) directions, t is time, p is pressure, and R is the Reynolds number U_0L/ν (U_0 is the freestream velocity, L is the plate length, and ν is kinematic viscosity). All quantities in the above equations are made dimensionless, using U_0, L, and density ρ in the usual way.

In the k-ϵ model, the three Reynolds stresses are related to the corresponding mean rates of strain by an isotropic eddy viscosity ν_t by

$$-\overline{uv}=\nu_t\left(\frac{\partial U}{\partial y}+\frac{\partial V}{\partial x}\right)$$

$$-\overline{uu}=\nu_t\left(2\frac{\partial U}{\partial x}\right)-\frac{2}{3}k$$

$$-\overline{vv}=\nu_t\left(2\frac{\partial V}{\partial y}\right)-\frac{2}{3}k \tag{3}$$

and the governing equations [the equation of continuity (4), the Reynolds equations (5) and (6), and the transport equations (7) and (8) for the turbulent kinetic energy k and its rate of dissipation ϵ] are written:

$$\frac{\partial U}{\partial x}+\frac{\partial V}{\partial y}=0 \tag{4}$$

$$\frac{\partial U}{\partial t}+\left(U-2\frac{\partial \nu_t}{\partial x}\right)\frac{\partial U}{\partial x}+\left(V-\frac{\partial \nu_t}{\partial y}\right)\frac{\partial U}{\partial y}+\frac{\partial p}{\partial x}+\frac{2}{3}\frac{\partial k}{\partial x}-\frac{\partial \nu_t}{\partial y}\frac{\partial V}{\partial x}-\frac{1}{R_U}\left(\frac{\partial^2 U}{\partial x^2}+\frac{\partial^2 U}{\partial y^2}\right)=0 \tag{5}$$

$$\frac{\partial V}{\partial t}+\left(U-\frac{\partial \nu_t}{\partial x}\right)\frac{\partial V}{\partial x}+\left(V-2\frac{\partial \nu_t}{\partial y}\right)\frac{\partial V}{\partial y}+\frac{\partial p}{\partial y}$$
$$+\frac{2}{3}\frac{\partial k}{\partial y}-\frac{\partial \nu_t}{\partial x}\frac{\partial U}{\partial y}-\frac{1}{R_V}\left(\frac{\partial^2 V}{\partial x^2}+\frac{\partial^2 V}{\partial y^2}\right)=0 \quad (6)$$

$$\frac{\partial k}{\partial t}+\left(U-\frac{1}{\sigma_k}\frac{\partial \nu_t}{\partial x}\right)\frac{\partial k}{\partial x}+\left(V-\frac{1}{\sigma_k}\frac{\partial \nu_t}{\partial y}\right)\frac{\partial k}{\partial y}$$
$$-\frac{1}{R_k}\left(\frac{\partial^2 k}{\partial x^2}+\frac{\partial^2 k}{\partial y^2}\right)-G+\epsilon=0 \quad (7)$$

$$\frac{\partial \epsilon}{\partial t}+\left(U-\frac{1}{\sigma_\epsilon}\frac{\partial \nu_t}{\partial x}\right)\frac{\partial \epsilon}{\partial x}+\left(V-\frac{1}{\sigma_\epsilon}\frac{\partial \nu_t}{\partial y}\right)\frac{\partial \epsilon}{\partial y}$$
$$-\frac{1}{R_\epsilon}\left(\frac{\partial^2 \epsilon}{\partial x^2}+\frac{\partial^2 \epsilon}{\partial y^2}\right)-c_{\epsilon 1}\frac{\epsilon}{k}G+c_{\epsilon 2}\frac{\epsilon^2}{k}=0 \quad (8)$$

where

$$G=\nu_t\left\{2\left(\frac{\partial U}{\partial x}\right)^2+2\left(\frac{\partial V}{\partial y}\right)^2+\left(\frac{\partial U}{\partial y}+\frac{\partial V}{\partial x}\right)^2\right\}$$

$$\nu_t=c_\mu\frac{k^2}{\epsilon}$$

$$\frac{1}{R_U}=\frac{1}{R_V}=\frac{1}{R}+\nu_t, \quad \frac{1}{R_k}=\frac{1}{R}+\frac{\nu_t}{\sigma_k}, \quad \frac{1}{R_\epsilon}=\frac{1}{R}+\frac{\nu_t}{\sigma_\epsilon}$$

$$C_\mu=0.09,\ \sigma_k=1.0,\ \sigma_\epsilon=1.3,\ c_{\epsilon 1}=1.44,\ c_{\epsilon 2}=1.92 \quad (9)$$

It should be noted that Eqs. (4–9) apply only to high Reynolds number, fully turbulent flows, and do not describe the flow in the near-wall region, where the direct influence of viscosity is important.

In the initial phase of this study, the so-called wall-function approach was employed to avoid the modeling of near-wall turbulence and solution of the equations in the sublayer and the blending zone. Our treatment of this is somewhat different, however, from what appears to be the standard practice. We explicitly require the first two grid points close to the wall, y_2 and y_3 in Fig. 1, to lie in the logarithmic law-of-the-wall region and use that requirement to determine the wall shear stress. Unlike most previous applications of wall functions, this procedure completely avoids the need for a separate analysis of the flow between the wall and the first grid point, $y_1<y<y_2$, $y_1=0$ being the wall. Specifically, a value of the friction velocity U_τ is assumed, and the velocity and turbulence quantities at y_2 are prescribed, in the usual manner, using the logarithmic law and the conditions of turbulence equilibrium, namely,

$$u^+=(1/\kappa)\ell n y^+ + B$$
$$k=U_\tau^2/\sqrt{C_\mu}$$
$$\epsilon=U_\tau^3/\kappa y \quad (10)$$

where $u^+=U/U_\tau$, $y^+=U_\tau y/\nu$, $\kappa=0.42$, and $B=5.5$. These boundary conditions enable the numerical solution to be obtained for $y>y_2$. The resulting velocity at the second grid node from the wall y_3 and the logarithmic law then provide a new value for the friction velocity to update the boundary conditions. Thus, an iterative procedure is used to enforce the wall functions and, typically, five iterations are required to obtain satisfactory convergence in U_τ.

A major advantage of this two-point formulation is that much of the sensitivity of the solutions to the location of the first grid point, which is found in other wall-function approaches,[4] is removed. Presumably, this is because the present method essentially requires both the velocity and its gradient to conform to the logarithmic law in the wall region. Further details and applications of this two-point wall-function method are given in Refs. 5 and 6.

While the above approach works satisfactorily for boundary layers and other wall-bounded flows, it is not adequate to resolve the very near wake. The innermost part of the near wake depends on the details of the flow in the sublayer and the buffer layer, which are not explicitly calculated. Therefore, within the spirit of the wall-function approach, one must exclude a region downstream of the trailing edge whose dimensions are of the order of y_2. This restriction, in turn, implies that the very large streamwise velocity gradients in the near wake cannot be resolved accurately and, therefore, the subsequent wake solution suffers from uncertainties in the initial conditions.

In order to resolve the interaction at the trailing edge at the same level of detail as achieved in laminar flow,[1] it is obviously necessary to incorporate the sublayer and the buffer layer in the solution procedure. An attempt was made first to use one of the low-Reynolds-number turbulence models, reviewed recently by Patel, Rodi and Scheuerer,[7] in which the constants of the k-ϵ model are replaced by damping functions to account for viscous and near-wall effects. This approach, however, was abandoned for the simple reason that none of the models reproduced the known characteristics of the mean flow in the wall region of a flat-plate boundary layer with sufficient accuracy to justify its use. This reconfirmed the observations made in Ref. 7. In view of the added numerical complexities of using low-Reynolds-number models and their less than satisfactory performance, it was decided to use a two-layer model, in which the standard k-ϵ model for the outer layer is combined with a simple but reliable eddy-viscosity model to describe the near-wall layer.

In the two-layer model, the computation domain is divided into two regions as shown in Fig. 1. Region I ($x\le 0$, $0\le y\le y_A$) includes the sublayer, the buffer layer, and a part of the logarithmic layer. A simple eddy-viscosity distribution is specified in this region so that the momentum equations can be solved using the no-slip boundary conditions at the wall. In region II, $y>y_A$, the standard k-ϵ model is employed to calculate the velocity field as well as the turbulence quantities. It should be remarked here that even with this approach, we are not properly modeling a small region just downstream of the trailing edge in which the upstream sublayers are destroyed. According to the analysis of Alber,[8] this region extends up to a distance of the order of 10 sublayer thicknesses. The numerical solutions with the present model are compared with Alber's theory to ascertain the influence of not incorporating any explicit damping in the turbulence model in this extreme inner wake.

In order to ensure a smooth distribution of eddy-viscosity and to provide an interaction between regions I and II, the wall shear stress (or friction velocity U_τ) is obtained in the same way as that in the wall-function approach, i.e., by applying the law of the wall at some $y=y_B$ located in the logarithmic region (say, $60<y^+<300$). Note that y_B, in

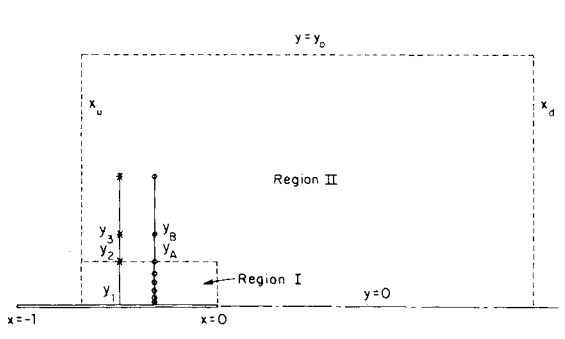

Fig. 1 Notation and solution domain: * grid for wall-functions; o grid for two-layer model.

general, need not coincide with y_A. In the present applications, y_B^+ in the neighborhood of 150 was used. Several y_A^+ values were tested, and the results were found to be insensitive to the location of this boundary between the two regions, provided it is in the logarithmic layer.

The distributions of the eddy-viscosity and the turbulence quantities in region I are specified by the following universal functions:

$$\nu_t = (1/2R)\,(\sqrt{1+4a^2}-1) \tag{11a}$$

$$a = \kappa y^+ [1-\exp(-y^+/A^+)], \qquad A^+ = 26.7 \tag{11b}$$

$$\begin{aligned} k^+ = \frac{k}{U_\tau^2} &= 0.05(y^+)^2, && y^+ < 5 \\ &= 1.25 + 0.325(y^+ - 5), && 5 < y^+ < 15 \\ &= 4.5 - (y^+ - 15)/37.5, && 15 < y^+ < 60 \\ &= 3.3, && 60 < y^+ < 150 \end{aligned} \tag{12}$$

$$\begin{aligned} \epsilon^+ = \frac{\nu\epsilon}{U_\tau^4} &= 0.1 + y^+/120, && y^+ < 12 \\ &= \frac{1}{\kappa y^+}, && y^+ > 12 \end{aligned} \tag{13}$$

The first is simply the well-known van Driest formula. The expressions for k and ϵ were derived from curve fits to the data summarized in Ref. 7. Note that k^+ in region I is needed not only to provide boundary conditions for k in region II but also for the evaluation of the source functions $\partial k/\partial x$ and $\partial k/\partial y$ in the momentum equations. On the other hand, ϵ^+ needs to be evaluated only on the boundaries of region II. Because all the functions in Eqs. (11-13) depend on the shear velocity U_τ determined from region II, a smooth variation of the turbulence quantities and eddy viscosity at the junction of the two regions is ensured.

III. Solution Procedures

The numerical method used for the solution of the equations presented in the last section is essentially the same as that employed for the laminar problem in Ref. 1. The principal differences between the previous and present applications of the method lie in the boundary conditions and the treatment of the two-layer turbulence model. In the present case, the numerical solution domain consists of regions I and II shown in Fig. 1, and the boundary conditions are as follows:

Upstream, $x = x_u$,	U, k^+, ϵ^+ specified; $V_x = 0$
Downstream, $x = x_d$,	$p_x = U_{xx} = V_{xx} = k_{xx} = \epsilon_{xx} = 0$
Outer, $y = y_0$,	$U = 1$, $k_y = \epsilon_y = p = 0$
Wake centerline, $y = 0$, $x > 0$,	$U_y = k_y = \epsilon_y = V = 0$
Plate, $y = 0$, $x < 0$,	$U = V = 0$
Region I, $y \le y_A$, $x \le 0$,	ν_t, k^+, ϵ^+ specified via U_τ determined from law of the wall at y_B

(14)

Note that simple symmetry conditions are employed along the wake centerline for the present problem. However, neither the numerical method nor the turbulence model is restricted to symmetric bodies. Also, when the wall-function approach is used, region I is excluded from the solution domain, and the last two boundary conditions are replaced by Eqs. (10).

It is perhaps worth noting at this stage that the present two-layer approach should not be confused with the parabolic sublayer (PSL) procedure suggested by Iacovides and Launder.[9] Here, we are concerned with the problem of using different models of turbulence in two different zones in the solution of the complete Reynolds-averaged equations

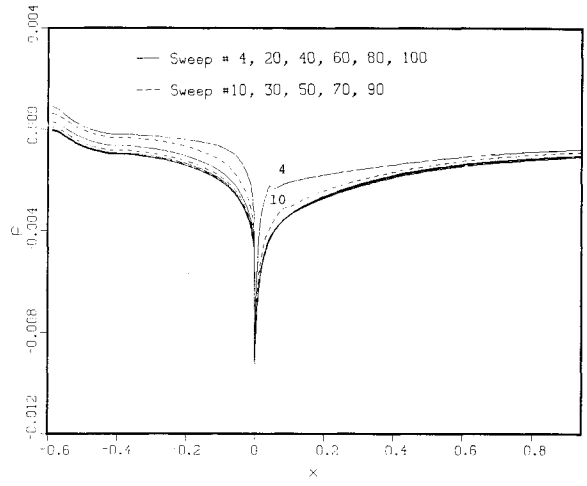

Fig. 2 Convergence of the pressure distribution.

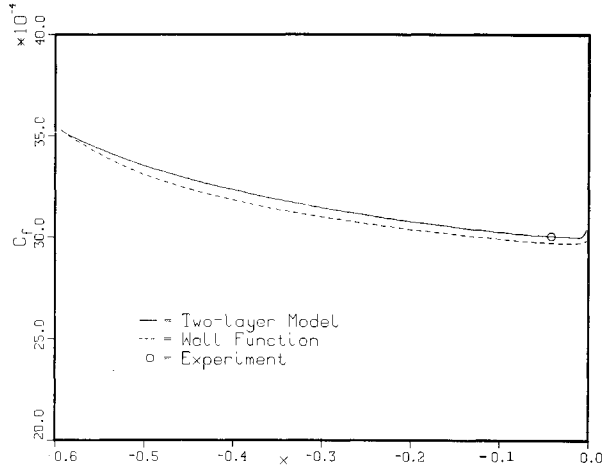

Fig. 3 Skin-friction coefficient.

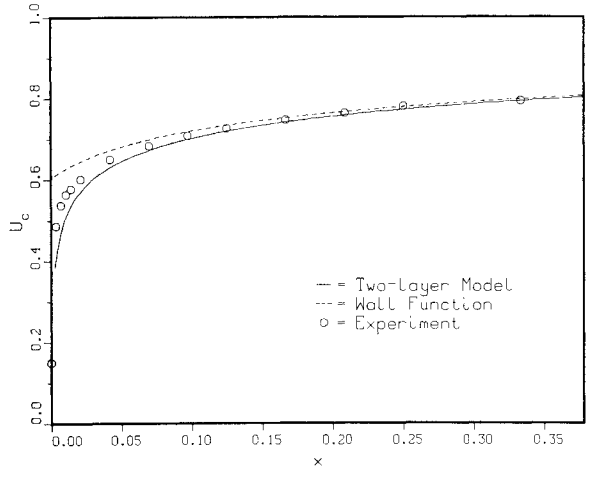

Fig. 4 Centerline velocity in the near wake.

of momentum and continuity. The PSL procedure, on the other hand, is concerned with approximations in the governing equations in the wall region. In the present scheme, numerical solutions for the elliptic velocity and pressure fields are obtained with the no-slip conditions specified on the plate and the zero-gradient boundary conditions imposed along the wake centerline. The turbulence quantities k and ϵ are computed from the differential equations only in region II. In this fashion, the near-wall layer and the central portion of the wake are resolved without a significant increase in computation time.

All the solutions presented below were obtained with the computation domain:

$$-0.6<x<8.57, \qquad 0<y<1.0$$

Extensive numerical tests, similar to those discussed at length in Ref. 1 for the laminar case, were conducted to ensure domain-size and grid independence of the solutions. The downstream boundary at $8.57L$ is sufficiently far in the wake to realize asymptotic conditions, and the outer boundary at L is more than sufficient to capture the viscous-inviscid interaction.

For the calculations with the two-layer turbulence model, a 57×25 nonuniform grid was employed with appropriate concentration of nodes near the trailing edge, and close to the plate and wake centerline. Of the 25 points in the y direction, up to 9 points lay in region I, with the first grid node located in the sublayer at y^+ as small as 0.4.

As noted earlier, calculations were also performed using the two-point wall-function approach. In order to facilitate a direct comparison of the results of the two approaches, the same solution domain was used, and a 57×16 grid, obtained simply by deleting the inner 9 nodes of the grid used in the two-layer calculations, was employed. Thus, referring to Fig. 1, $y_2=y_A$. For the Reynolds number considered here, this arrangement puts the first grid node at $y_2^+\sim100$.

One of the important features of the time-marching numerical scheme employed here is that, for steady flows, it provides a rapid and monotonic convergence to the final solution with very simple initial conditions and quite large time steps. This was demonstrated in Ref. 1 with laminar flow. Figure 2 shows the convergence of the pressure distribution on the plate and along the wake centerline, starting with zero pressure throughout the solution domain, in the present calculations with the two-layer model. It is clear that satisfactory convergence is obtained in about 50 time steps or iterations. Other quantities, such as wall shear stress and wake centerline velocity, also converge in less than 50 iterations. The convergence properties are not affected by the use of wall functions.

IV. Results and Discussion

Calculations have been performed for a plate of length $L=1.829$ m in an airstream of velocity $U_0=22$ m/s, so that the Reynolds number $R=U_0L/\nu=2.48\times10^6$. These conditions correspond to the experiments of Ramaprian et al.,[2] who made mean-velocity and turbulence measurements in the region $-0.0417<x<0.333$ ($-76.2<X<609.6$ mm, where X is the physical distance from the trailing edge). Solutions of the boundary-layer equations for the near and far wake, with the same turbulence model (and model constants) as used here, have been presented by Patel and Scheuerer.[3] The results of the present calculations will be compared with the experiments, the previous noninteractive calculations, and the analytical results of Alber,[8] which are also based on boundary-layer assumptions.

The converged pressure distribution shown in Fig. 2 provides an overview of the interaction at the trailing edge. A sharp reduction, followed by a rapid increase in pressure, is predicted near the trailing edge. Comparison of these results with the corresponding ones for laminar flow in Ref. 1 (Fig. 10a) indicates that the viscous-inviscid interaction in turbulent flow is weaker, as measured by the pressure changes, but extends to a much larger distance downstream of the trailing edge. The slower recovery of the wake centerline pressure to the ambient value is related to the Reynolds stress $\overline{vv}$, as will be discussed later.

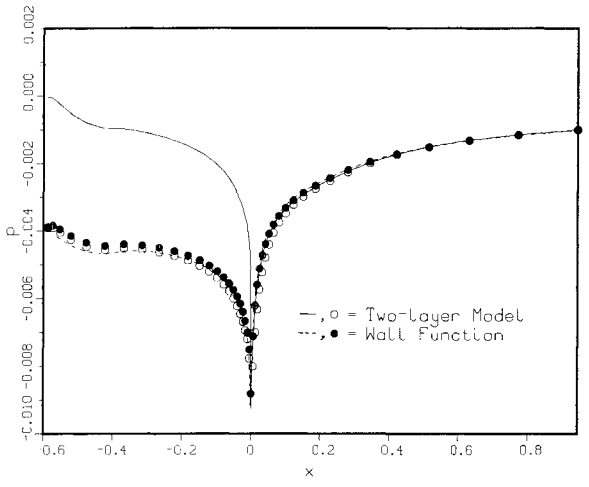

Fig. 5 Pressure distribution on the plate and along wake centerline. Lines: $y=0$; symbols: $y^+\sim100$.

For clarity, it is useful to present and discuss the results in the following order: first, we consider the difference between the wall-function and the two-layer approaches, as well as the overall interaction at the trailing edge; then, we examine the details of the flow in the near wake; and finally, we consider the approach to asymptotic conditions in the far wake. For the analysis of the evolution of the wake from the boundary layer, it is convenient to introduce a nondimensional distance from the trailing edge, $x^+=U_{\tau0}x/\nu$, where $U_{\tau0}$ is the trailing-edge friction velocity. In a similar vein, velocity distributions across the near wake are analyzed in terms of the variables $u^+=U/U_{\tau0}$ and $y^+=U_{\tau0}y/\nu$. We distinguish between these and the usual wall variables in the boundary layer only when necessary.

Figures 3-5 show, respectively, the wall shear stress ($C_f=2U_\tau^2$), the mean velocity along the wake centerline (U_c), and the pressure distribution on the plate and along the wake centerline, predicted by the two sets of calculations. The available data from Ref. 2 are included in the first two figures. Systematic differences are observed between the results of the two treatments of the flow in the near-wall region.

As might be expected from the underlying assumptions, the differences in the wall shear stress are the smallest, being at most of the order of 1%. If these are disregarded, an increase in wall shear stress is predicted near the trailing edge by both methods. This is associated with a local acceleration of the flow, but neither the magnitude of the increase nor its streamwise extent is as large as that in laminar flow.[1] Thus, the viscous-inviscid interaction at the trailing edge in turbulent flow is weaker, and its upstream extent, in terms of plate lengths, is smaller. A more meaningful measure of this extent, however, is $x^+\sim250$, or 25 sublayer thicknesses.

The difference between the two solutions are quite large in the distribution of the wake centerline velocity, shown in Fig. 4. The wall-function approach predicts a much faster increase in velocity in the near wake than that indicated by the data. This may result from two factors: the absence of the sublayer and the buffer layer in the model and, associated with the wall-function approach, a rather coarse grid in this region of large gradients. The two-layer model, on the other hand, predicts a slower increase in centerline velocity, but the general trend of the experimental results is modeled correctly. Also, as we shall see later from more detailed velocity

comparisons, the measurements in the neighborhood of the wake centerline may be somewhat higher than expected from theoretical considerations.

Figure 5 shows the streamwise distribution of pressure along two lines: 1) on the plate and along the wake centerline, $y=0$, and 2) along y_A ($y^+ \sim 100$), which separates the two regions in the two-layer model and along which the wall functions are applied. We note that nearly identical results are obtained with the two approaches for the pressure distribution along the latter line although quite different distributions are pedicted at the plate itself. In order to understand this, it is necessary to examine Fig. 6, which shows the details of the variation of pressure normal to the plate at several locations in the neighborhood of the trailing edge. In the wall-function approach, the surface pressure is obtained simply by an extrapolation (linear for $x<0$ and second-order symmetric for $x>0$) of the numerical solution and, therefore, little variation of pressure is predicted across the wall layer. In the two-layer approach, the pressure is calculated all the way to the wall, and significant variation of pressure across the buffer layer and the sublayer is observed. At first sight, this result is surprising, but examination of the y-momentum equation (2) shows that, in the near-wall region, pressure variation is to be expected owing to the variations in the Reynolds normal stress $\overline{vv}$ which, in turn, is related to the turbulent kinetic energy k through the isotropic eddy-viscosity assumption, i.e.,

$$\frac{\partial p}{\partial y} \approx -\frac{\partial \overline{vv}}{\partial y} \approx -\frac{2}{3}\frac{\partial k}{\partial y} \tag{15}$$

In other words, we expect a minimum in pressure at $y^+ = 15$, where the prescribed distribution of k^+ reaches a maximum. This is indeed what is seen in Fig. 6.

From the results for the pressure distributions shown in Figs. 5 and 6 we can make the following observations. First, we see that the influence of the normal-stress term in the equations of motion is not small. Because the calculations are based on the assumption of an isotropic eddy viscosity, which does not take into account the extra damping of the normal stress $\overline{vv}$ (compared with the other components) close to the wall, a somewhat higher wall pressure is predicted by the two-layer model. Second, the longitudinal pressure gradients on the plate calculated by both approaches are very small, except in the neighborhood of the trailing edge. This result confirms the validity of boundary-layer approximations over most of the plate, as well as the observation made earlier that the trailing-edge interaction in turbulent flow does not penetrate as far upstream as in the laminar case. Finally, we note that the influence of the normal stresses, which appears to be significant in the present weak-interaction problem, is unlikely to be very important in more practical trailing-edge geometries, where pressure variation due to streamline curvature is of much greater significance.

Thus far, only the overall parameters of the flow have been considered. The results are shown in somewhat greater detail in Figs. 7 and 8, where the two sets of calculations are compared with the measured velocity and turbulent kinetic-energy profiles at several distances from the trailing edge, X and x/θ, where θ is the total momentum thickness of the wake made dimensionless by the plate length L. It is observed that both approaches provide quite satisfactory descriptions of the boundary layer and wake except in the central portion of the near wake. The observed differences in the near wake are directly related to the treatment of the flow in the near-wall layer. Use of the wall-function approach, together with the attendant problem of inadequate grid concentration, results in the prediction of greater centerline velocity and lower turbulent kinetic energy. The two-layer model provides a much improved description, especially with respect to the turbulent kinetic energy,

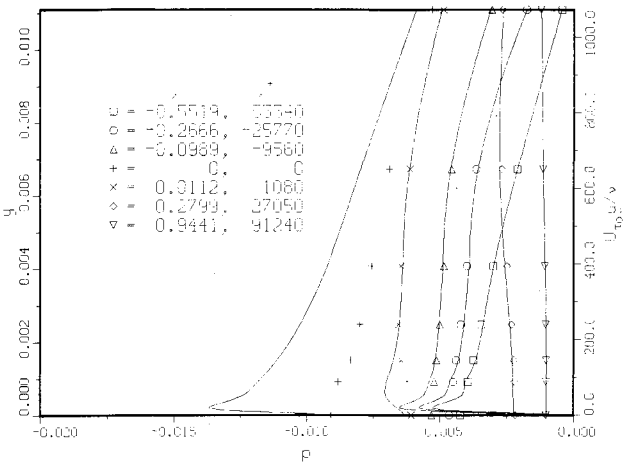

Fig. 6 Pressure variation in the normal (y) direction. Lines: two-layer model; symbols: wall functions.

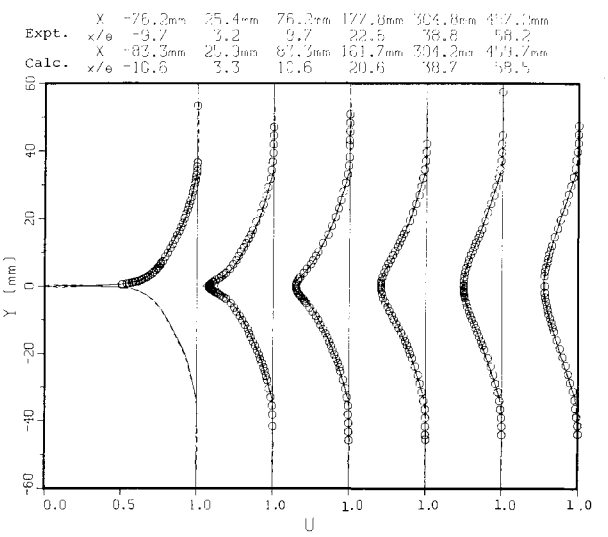

Fig. 7 Velocity profiles in the near wake: o experiment; —— two-layer model; - - - - wall functions.

although, as already noted from Fig. 4, the velocity data lie somewhat higher than the calculations.

A much more detailed picture of the flow near the trailing edge is obtained by examining the results with the two-layer model in wall-layer coordinates and making comparisons with the theory of Alber.[8] First of all, the overall success of the two-layer model for the boundary layer is illustrated in Fig. 9. It is clear that the solutions of the complete Reynolds equations with the prescribed eddy viscosity faithfully reproduce the sublayer and buffer regions. Also, the scheme adopted to maintain continuity of the prescribed eddy viscosity in the wall layer with that deduced from the numerical solution of the k-ϵ model equations, i.e., determining the wall shear from the logarithmic law, appears to be quite effective insofar as a smooth velocity profile is predicted throughout the boundary layer. A close examination of the profiles in Fig. 9 indicates that a universal inner layer is calculated everywhere except at the station close to the trailing edge. In fact, the departure from the unique profile is consistent with the effect of the locally favorable pressure gradient, induced by the trailing-edge interaction, on the sublayer. Thus, the two-layer calculations are able to capture the details of the interaction in the sublayer. It is also clear that this cannot be accomplished with the wall-function approach.

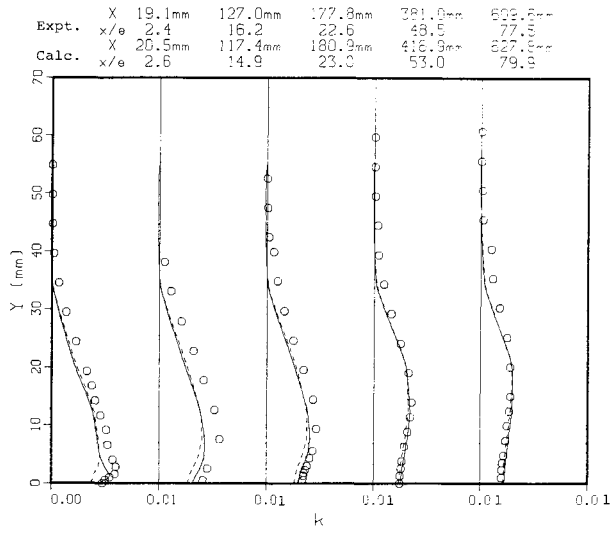

Fig. 8 Turbulent kinetic-energy distributions in the near wake: o experiment; —— two-layer model; - - - - wall functions.

Alber has presented similarity solutions of the boundary-layer equations for the central portion of the near wake. Assuming that the wall region of the upstream boundary layer can be described in two parts, namely, a laminar sublayer and a logarithmic layer, Alber showed that a laminar inner wake exists just downstream of the trailing edge in which the sublayers are destroyed, and a turbulent inner wake farther downstream in which the logarithmic layers are destroyed. The laminar inner wake follows the well-known Goldstein solution, i.e.,

$$u_c^+ = 1.611(x^+)^{1/3} \tag{16}$$

where $u_c^+ = U_c/U_{\tau 0}$. Under the assumption of a linear distribution of eddy viscosity in the normal direction, the velocity field in the turbulent inner wake is given by

$$u_c^+ = \frac{1}{\kappa}[\ln g(x^+) - \gamma] + B \tag{17}$$

$$u^+ = \frac{1}{\kappa}[\ln y^+ + E_1(\zeta)] + B \tag{18}$$

where

$$\zeta = \frac{y^+}{g(x^+)}, \qquad E_1(\zeta) = \int_\zeta^\infty \frac{e^{-t}}{t}\,dt$$

$$g(\alpha)[\ln g(\alpha) - 1] = \kappa^2 \alpha \tag{19}$$

and γ (=0.5772157) is the Euler constant. In the present study, the constants in Eqs. (17) and (18) were taken as $\kappa = 0.42$ and $B = 5.5$ for consistency with the constants used in the turbulence models.

Ramaprian et al.[2] presented comparisons between their wake data and the theory of Alber. Here, we shall compare the present numerical solutions with the experimental data and Alber's theory. The principal results are shown in Figs. 10 and 11.

From Fig. 10, which shows the distribution of velocity along the wake centerline, it is evident that the numerical solution reproduces all the essential features of the theory. In particular, the present solution agrees with the laminar equation (16), provides a smooth transition between this and the logarithmic turbulent inner wake, agrees with the turbulent formula (17) over the range $3000 < x^+ < 30{,}000$, and even-

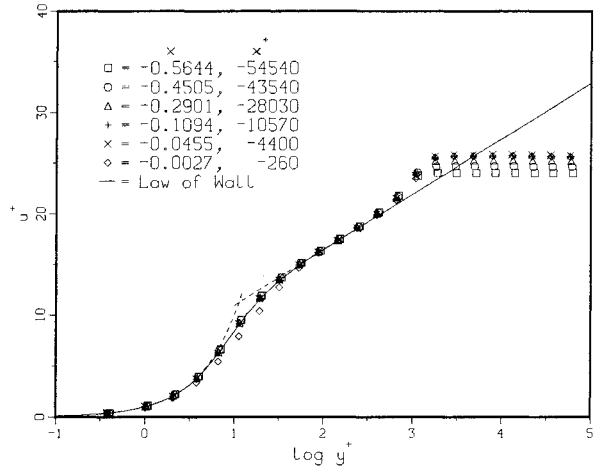

Fig. 9 Velocity profiles in boundary layer in wall coordinates.

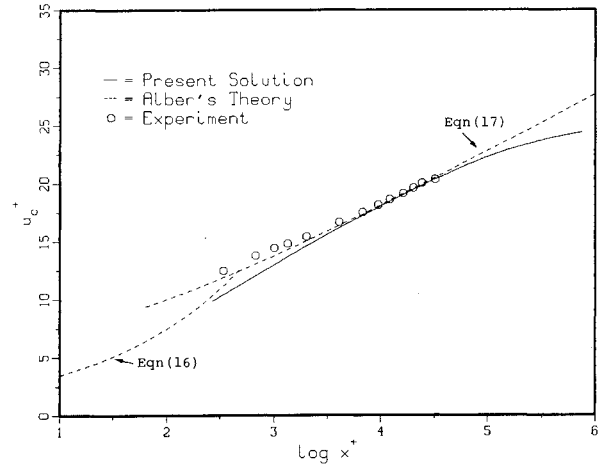

Fig. 10 Wake centerline velocity in wall coordinates.

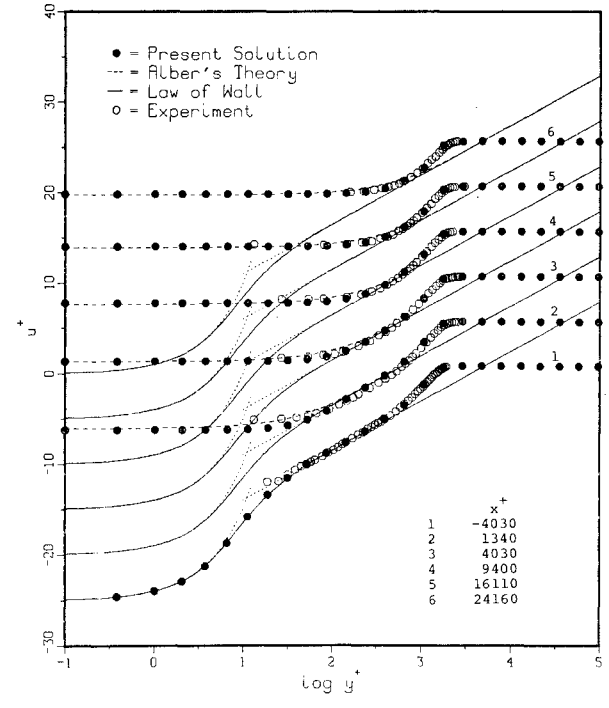

Fig. 11 Near-wake velocity profiles in wall coordinates.

tually diverges from the logarithmic formula to indicate an asymptotic behavior. The experimental data are in agreement with the turbulent formula even in what appears to be the transition zone from the laminar to the turbulent relation. The reason for this is not entirely clear, but two explanations are possible. The first is that the pitot-probe data very close to the trailing edge may be influenced by the high shear and turbulence, since both effects would tend to indicate higher velocities. The second is that there is indeed a faster mixing in the near wake and that it is not modeled accurately either by Alber's theory or by the present two-layer approach. In this regard, we note that Alber assumed a linear distribution of eddy viscosity, with a value of zero at the wake center, across the turbulent inner wake. On the other hand, the present work uses the standard k-ϵ model in the wake and, therefore, does not explicitly account for any damping in the laminar or transitional portions of the near wake. In the present calculations, however, the laminar region in the wake is not resolved with the grid arrangement employed but, as evidenced by Fig. 9, the initial conditions in the upstream boundary layer are resolved quite accurately.

The detailed velocity profiles in the near wake are compared in Fig. 11. It is quite evident that the present solution is in almost complete agreement with Alber's theory in spite of the differences noted above. The calculations are also in excellent agreement with the experiments with the possible exception of the small region close to the wake center. The rapid destruction of the sublayer and the somewhat slower erosion of the logarithmic layers are clearly shown. Figures 10 and 11 together indicate that the sublayers are destroyed by about $x^+ = 250$ and remnants of the logarithmic layers are present up to $x^+ = 30{,}000$.

From the near wake, we now turn our attention to the far wake. The assumptions of self-preservation and small velocity defect ($w = 1 - U \ll 1$) in the far wake lead to the well-known half-power laws for the decay of the centerline velocity defect W_0 ($= 1 - U_c$), the growth of the half-width b ($= 2y$ where $W/W_0 = 1/2$). The approach of the centerline velocity defect to the half-power law in the far wake is shown in Fig. 12, along with the far-wake data of Pot.[10] The calculated distribution of the wake centerline eddy viscosity is also included. It is clear that the calculations with the wall functions and two-layer model for the boundary layer yield only slightly different results in the wake. It is believed that these differences are due more to the differences in the numerical grids than to a genuine effect of the upstream boundary conditions. Recall that nine additional grid points are employed near the wake centerline in the two-layer formulation while the remaining grid is the same.

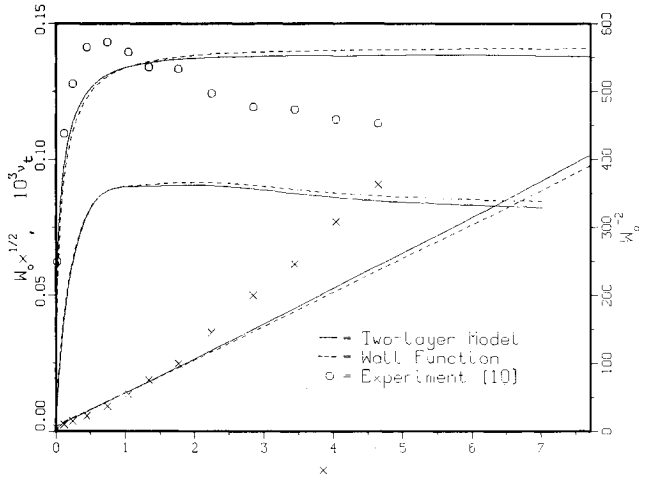

Fig.12 Wake centerline velocity defect and eddy-viscosity: approach to asymptotic state.

Figure 12 indicates that similarity is established beyond a distance of about two plate lengths ($x > 2$) from the trailing edge. This corresponds to about 500θ, a somewhat greater distance than the 350θ suggested in Ref. 2. Although there is substantial agreement in the distance required for the establishment of asymptotic conditions, Fig. 12 shows that the calculations do not predict the overshoot of $W_0 x^{1/2}$ observed in the experiments, and the calculated asymptotic value is about 25% higher. This higher value is consistent not only with the slower rate of decay of the velocity defect but also with the predicted eddy viscosity. The calculated centerline eddy viscosity increases rapidly in the near wake, unlike the assumption of Alber, reaches a nearly constant value ($\nu_t = 0.000091$) in the region $1.0 < x < 2.5$, and then decreases very slowly in the far wake. The above value of ν_t corresponds to $\nu_t/\theta = 0.022$, which is about 30% lower than the experimental value of 0.032.[2,3]

The far-wake features of the present solutions, namely, lower eddy viscosity and slower rate of decay of the velocity defect, as well as the shapes of the velocity-defect and stress profiles, which are not presented here, are all in general agreement with the previous results of Patel and Scheuerer.[3] This is not surprising since the same turbulence model, with the same constants, was employed. It is, however, of interest to note the very significant differences between the two solution procedures. First, the calculations of Ref. 3 employed the parabolic boundary-layer equations and were started at the trailing edge. Thus, neither the upstream boundary layer nor the viscous-inviscid interaction at the trailing edge were considered. These details are captured by the present solution, particularly with the two-layer formulation, which improves the resolution of the flow close to the plate and in the very near wake. Although the differences between the present solutions and those of Ref. 3 may appear to be small when viewed in the format of Figs. 7 and 8, some systematic differences exist. For example, the slightly lower eddy viscosity predicted by the present method may be attributed to the retention of all the turbulent stresses in the Reynolds equations, whereas the somewhat slower increase of the wake centerline velocity is consistent with the adverse pressure gradient that exists in the wake. Computationally, the two methods are also very different. Reference 3 employed a traditional parabolic marching scheme and used 60 points across the wake and 800 streamwise steps in the region $0 < x < 0.3$ to achieve acceptable accuracy. The present method, on the other hand, required only a 57×25 grid over a very much larger solution domain, $-0.6 < x < 8.6$, $0 < y < 1.0$, which includes the boundary layer, the near and far wakes, and the external inviscid flow.

V. Conclusions

Numerical solutions of the Reynolds-averaged Navier-Stokes equations have been obtained for the flow in the turbulent boundary layer and in the near and far wake of a flat plate using a large computation domain. The k-ϵ model of turbulence, with generally accepted constants, has been used in regions away from the solid wall, as in previous studies. In the near-wall region, however, a prescribed eddy-viscosity distribution is employed to account for the effects of wall proximity and viscosity. Comparisons with the wall-function approach, which avoids direct modeling of near-wall turbulence, indicate that this two-layer model enables quite accurate resolution of the sublayer and the buffer layer on the plate, and the central portion of the wake, without significant increase of computation time. More sophisticated turbulence models can be incorporated easily in the proposed two-layer approach to account for the direct influence of wall roughness, body curvature, pressure gradient, etc.

The present large-domain solution is in good agreement with experiments and with Alber's near-wake theory. The rate of decay in the asymptotic wake is underpredicted, as has been noted on previous occasions on the basis of bound-

ary-layer equations. Modifications in the k-ϵ model are obviously needed in order to improve the prediction of the asymptotic wake.

Acknowledgments

This research was supported by the Office of Naval Research under the Accelerated Research Initiative (Special Focus) Program in Ship Hydrodynamics, Contract N00014-83-K-0136.

References

[1]Chen, H. C. and Patel, V. C., "Laminar Flow at the Trailing Edge of a Flat Plate," *AIAA Journal*, Vol. 25, July 1987, pp. 920–928.

[2]Ramaprian, B. R., Patel, V. C., and Sastry, M. S., "The Symmetric Turbulent Wake of a Flat Plate," *AIAA Journal*, Vol. 20, Sept. 1982, pp. 1228–1235.

[3]Patel, V. C. and Scheuerer, G., "Calculation of Two-Dimensional Near and Far Wakes," *AIAA Journal*, Vol. 20, July 1982, pp. 900–907.

[4]Rubesin, M. W. and Viegas, J. R., "A Critical Examination of the Use of Wall Functions as Boundary Conditions in Aerodynamic Calculations," *Proceeding of the 3rd Symposium on Numerical and Physical Aspects of Aerodynamic Flows*, Long Beach, CA, Jan. 1985.

[5]Chen, H. C. and Patel, V. C., "Calculation of Trailing-Edge, Stern and Wake Flows by a Time-Marching Solution of the Partially-Parabolic Equations," Iowa Institute of Hydraulic Research, The University of Iowa, Iowa City, IA, IIHR Rept. 285, 1985.

[6]Chen, C. J., Yoon, Y. H., and Yu, C. H., "The Finite Analytic Method," Iowa Institute of Hydraulic Research, The University of Iowa, Iowa City, IA, IIHR Rept. 232-VI, 1983.

[7]Patel, V. C., Rodi, W., and Scheuerer, G., "Turbulence Models for Near-Wall and Low Reynolds Number Flows: A Review," *AIAA Journal*, Vol. 23, Sept. 1985, pp. 1308–1319.

[8]Alber, I. E., "Turbulent Wake of a Thin, Flat Plate," *AIAA Journal*, Vol. 18, Sept. 1980, pp. 1044–1051.

[9]Iacovides, H. and Launder, B. E., "PSL—An Economic Approach to the Numerical Analysis of Near-Wall, Elliptic Flow," *Journal of Fluids Engineering*, Vol. 106, June 1984, pp. 241–242.

[10]Pot, P. J., "Measurements in a 2-D Wake and a 2-D Wake Merging into a Boundary Layer," Data Report, The Netherlands, NLR TR-79063 U, 1979.